

Temperature versus salinity: distribution of stratification control in the global ocean

Romain Caneill¹ and Fabien Roquet¹

¹Department of Marine Sciences, University of Gothenburg, Gothenburg, Sweden

Correspondence: Romain Caneill (romain.caneill@gu.se)

Abstract. The ocean stratification is controlled by temperature in subtropical regions (alpha oceans), by salinity in polar regions (beta oceans), and by both in the transition zones. The polar transition zone (PTZ) is located in between subtropical alpha and polar beta oceans. The PTZ exists in the North Pacific, North Atlantic, and Southern Ocean, despite different circulations and oceanic properties between them. Deep winter mixed layers (MLs) are found in the vicinity of the PTZ, which makes it a key component to link the surface and the ocean interior. The global climatological state and the variability from the climatology are not fully described in previous studies studying control of stratification. Based on observational temperature – salinity profiles, we compute novel climatologies of the stratification below the ML, classifying the global oceans into alpha, beta, or transition zones. Using the profiles, we also computed a monthly product for every year between 2004 – 2021, allowing for the study of interannual variability. On the climatological state, we describe accurately the PTZ between subtropical alpha ocean and polar beta ocean. Our study highlights the difference between each basin: the alpha ocean stops at 40°N in the Pacific basin, but reaches 80°N in the eastern part of North Atlantic. In both the North Atlantic and Southern Oceans, the PTZ is narrow, while in the east-north Pacific Ocean it spans 20 degrees of longitude. The SO Subantarctic and Polar Fronts are located at the shifts between the stratification regimes.

1 Introduction

Temperature and salinity vary differently with depth in the subtropics and in polar regions. Taking a transect between Australia and Antarctica reveals two opposite regimes (Fig. 1). In the subtropical part, temperature and salinity both decrease with depth, while in the polar part, temperature and salinity increase with depth. In between the subtropical and polar regimes exists a narrow region where temperature decreases with depth, and salinity increases. As warm and fresh water is lighter than cold and salty water, stratification of the upper ocean is thus controlled by temperature in the subtropics and salinity in the polar regions (Pollard et al., 2002; Carmack, 2007). These two different types of stratification are called alpha (stabilised by temperature) and beta (stabilised by salinity) oceans, respectively (Carmack, 2007). In between these regions lies the polar transition zone (PTZ), where both temperature and salinity increase stratification (Caneill et al., 2022). Tropical oceans at the equator are also stratified by temperature and salinity (Clément et al., 2020). The transition from an alpha ocean in subtropical regions through a transition zone to a beta ocean in polar regions is a notable characteristic observed both in the Northern and Southern Hemisphere (Pollard et al., 2002; You, 2002; Carmack, 2007; Stewart and Haine, 2016).

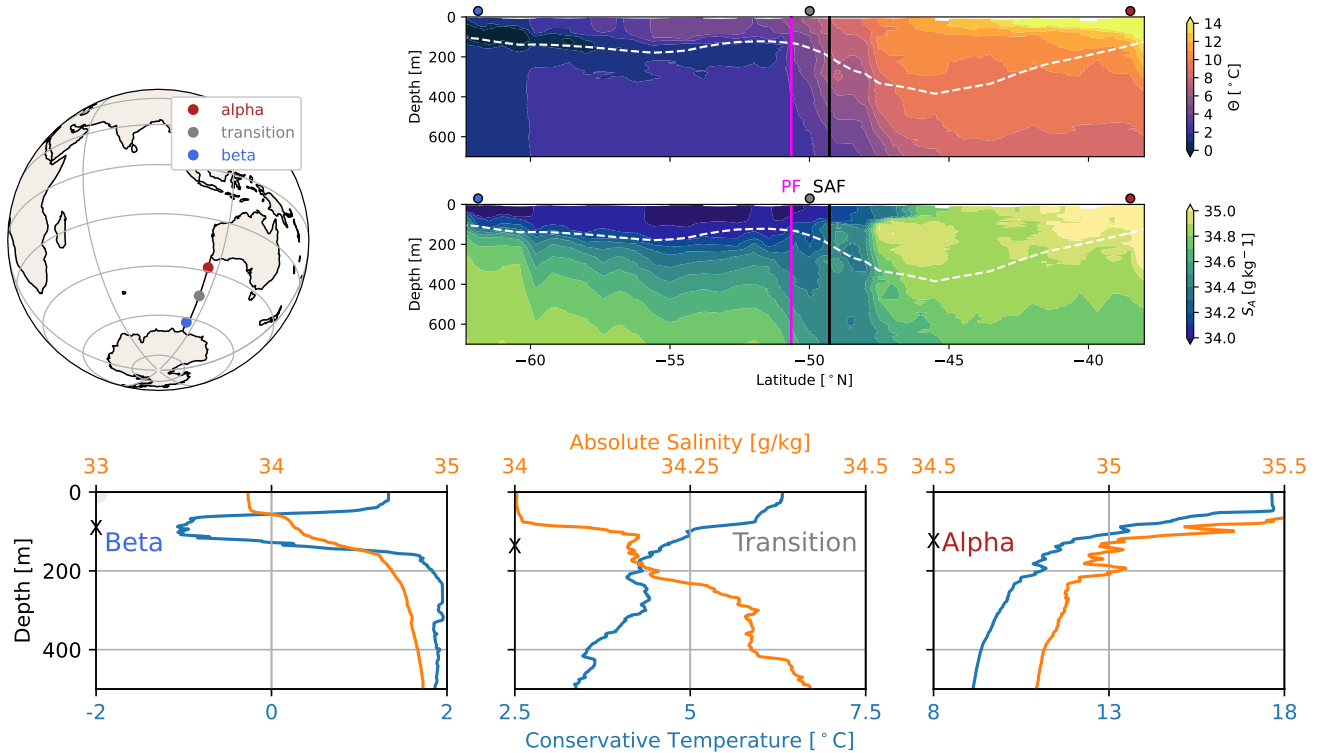


Figure 1. Temperature and salinity sections along the IO9S transect. Data are from the hydrographic cruise 09AR20120105 (CCHDO Hydrographic Data Office, 2023). The vertical lines mark the boundaries of, from north to south, alpha ocean, transition zone, and beta ocean. These boundaries are determined by the Subantarctic Front (SAF, black line) and the Polar Front (PF, purple line). The white and dashed line represents the climatological winter mixed layer depth (from (de Boyer Montégut, 2023)). The three bottom panels correspond to the three dots of the upper panels. The black crosses on the left vertical axes represent the climatological winter mixed layer depth.

The alpha – beta distinction reveals important implications. The halocline present in beta ocean is essential for sea-ice formation (Carmack, 2007). Simultaneously, the increase of temperature with depth maintains a heat reservoir, which can damp the formation of sea-ice, melt it, and contribute to deep convection events (Martinson et al., 1981; Pierce et al., 1995; Martin et al., 2013; Polyakov et al., 2013). Reduced sea-ice under warmer conditions lowers ocean albedo, increasing heat absorption and further amplify ocean warming (Curry et al., 1995; Perovich and Polashenski, 2012).

Winter mixed layers in temperature-stabilised regions are generally deeper than in salinity-stabilised ones, allowing beta ocean to re-stratify faster in summer (Carmack, 2007). Double diffusive effect arise in alpha and beta ocean, but not transition zone where both temperature and salinity stabilise the water column (Stern, 1960; Schmitt, 1994; You, 2002).

The existence of the polar transition zone in all subpolar oceans indicates that intrinsic properties of seawater could drive the alpha / beta distinction (Carmack, 2007). Roquet et al. (2022) showed that the existence of beta ocean is possible because

the thermal expansion coefficient becomes small in cold water. This makes the density of cold seawater almost insensitive to temperature. Moreover, polar regions undergo large surface freshwater input, which form the halocline. If the thermal expansion were larger, the halocline could not exist in winter due to heat loss driven convection (Roquet et al., 2022; Caneill et al., 2023, manuscript submitted to Ocean Science).

40 The characteristics of the PTZ vary however between the different basins. In the North Pacific Ocean, the PTZ is associated with a surface density maximum (Roden, 1970; Stewart and Haine, 2016; Johnson et al., 2012). This density maximum is however not found in the Southern Ocean (SO) PTZ: the density maximum is located close to the coast of Antarctica, in beta ocean.

In the SO, the transition from subtropical to polar waters is achieved by a succession of fronts part of the Antarctic Circumpolar Current (ACC). Three fronts have been historically defined based on thermohaline properties: from north to south the Subantarctic Front (SAF), the Polar Front (PF), and the Southern ACC front (SACCF). The Polar Frontal Zone (PFZ) is the zone of change between Antarctic and Subantarctic surface waters. The PFZ is a permanent feature in the SO (Emery, 1977), that exists by definition everywhere in the SO. Pollard et al. (2002) proposed to define the SAF and PF based on stratification, which directly relates to the concept of alpha and beta ocean: the SAF marks the boundary between alpha ocean and the PTZ, while the PF marks the boundary between the PTZ and the beta ocean. The boundary between regions of different thermohaline structure are thus used as definition for the fronts (Pauthenet et al., 2017; Thomas et al., 2021).

The position of the PF is associated with a strong ocean jet (e.g. Trathan et al., 1997). With more observations available (both in situ and from satellite) it became more common to consider that the ACC is made of multiple frontal filaments (Sokolov and Rintoul, 2009). Dynamic fronts are located at the position of strong jets and strong isopycnal slopes or sea surface height (SSH) gradient. Dynamic fronts can be transient, so a definition based on SSH gradient is more accurate than definitions following a SSH contour (Graham et al., 2012).

The control of stratification by temperature or salinity below the mixed layer (ML) usually varies depending on the season and location (Helber et al., 2012; Pellichero et al., 2017; DuVivier et al., 2018). The export of the ML properties to the interior happens when the ML is deepest and water escapes by lateral subduction (Sallée et al., 2010). The stratification control index (SCI) provides information on the relative effect of temperature and salinity on stratification, allowing to classify water masses in alpha, beta, or transition zone (Caneill et al., 2022; Roquet et al., 2022).

$$SCI = \frac{N_{\Theta}^2 - N_S^2}{N_{\Theta}^2 + N_S^2} \quad (1)$$

$$N^2 = -\frac{g}{\rho_0} \frac{\partial \rho_{\Theta}}{\partial z} = N_{\Theta}^2 + N_S^2 \quad (2)$$

$$N_{\Theta}^2 = g\alpha \frac{\partial \Theta}{\partial z} \quad (3)$$

$$65 \quad N_S^2 = -g\beta \frac{\partial S_A}{\partial z}. \quad (4)$$

It quantifies the relative effect of temperature and salinity on stratification, and is defined only for positive N^2 . Based on the SCI, 3 regions are defined:

1. $SCI > 1$: alpha ocean where temperature (salinity) increases (decreases) stratification;
2. $-1 < SCI < 1$: transition zone where temperature (salinity) increases (increases) stratification;
- 70 3. $SCI < -1$: beta ocean where temperature (salinity) decreases (increases) stratification.

The SCI below the winter ML informs on the stratification properties of the permanent pycnocline that links the intermediate ocean with the surface. DuVivier et al. (2018) remarked that subsurface salinity maximums in the SO are misrepresented in Earth System Models, which in return lead to biases in mixed layer depth (MLD) compared to observations. Knowing whether temperature or salinity are stabilising the water column below the ML is of main importance to understand the exchange of
75 properties (heat, salt, carbon, etc) between the surface and the interior.

Based on observational temperature – salinity profiles, we produce climatologies of the MLD and SCI for the different seasons. Following Pollard et al. (2002) and Carmack (2007) we thus use the thermohaline stratification to describe both the global oceans and the Southern Ocean. The description of the winter SCI provides a picture of the ocean that is both novel and at the same time coherent with previous descriptions. The paper is organised as follows: we first describe the EN.4.2.2 database
80 and the methods we used to produce the MLD and SCI climatologies. Then, we present the results of the mean climatological state along with the seasonal variations for both the global ocean before focusing on convective regions in the SO and Irminger Sea. Finally, we provide more detailed analysis in the SO, and finish with discussion and conclusions.

2 Material and Methods

This study uses a database of profiles of temperature and salinity to compute the MLD and SCI for each individual profiles.
85 Interpolation is then done to create both a gridded product, and a gridded monthly climatology.

2.1 EN4

The profiles are taken from the EN.4.2.2 (Good et al., 2013) ensemble members using Gouretski and Cheng (2020) MBT, and Gouretski and Reseghetti (2010) XBT corrections. Data from 2004 to 2021 are used. 2004 is the beginning of the ARGO era in the Southern Ocean, so we chose this lower limit to exclude years with too few measurements.

90 Data from EN4 have been filtered to remove badly flagged profiles. The profiles have been individually smoothed and re-sampled vertically following this algorithm, similar to (Johnson et al., 2002):

1. interpolate linearly along an evenly spaced grid with a resolution of 1 m, going from 0 to 2000 m;
2. smooth by applying the convolution with a hanning window (= a positive half sinus) with a window length of 20 m
3. interpolate linearly to a lower resolution vertical grid: every 5 m from 0 to 100 m, then every 10 m up to 350 m, then
95 every 25 m up to 500 m, and then every 50 m to 2000 m.

Fig. A1 in Appendix A presents a profile before and after smoothing. Small scale variations are removed, while keeping the global shape of the temperature profile.

2.2 Methods

2.2.1 MLD and SCI

100 We compute the MLD using a density threshold criteria of 0.03 kg m^{-3} (de Boyer Montégut, 2004; Sallée et al., 2021).
The SCI is computed between 10 and 30 m under the ML.

2.3 Interpolation on a regular grid

The gridding of the variables extracted from the profiles (MLD or SCI) is done using a radial basis function (RBF) interpolation. The class `scipy.interpolate.RBFInterpolator` from the Python `scipy` library is used.

105 To account for the anisotropy between the longitude and latitude scale factors, the latitude is transformed by a Mercator projection, using the following formula:

$$\varphi' = \ln\left(\tan\left(\frac{\varphi}{2} \frac{\pi}{180} + \frac{\pi}{4}\right)\right) \cdot \frac{180}{\pi} \quad (5)$$

This will virtually increase the difference of latitude between 2 points located in polar regions. To achieve isotropy, 2 points separated by the same geographical distance (i.e. measured in meter) along longitude or latitude should get the same distance
110 (Eq. (6) in a following paragraph). The difference of longitude is larger than the difference of latitude due to the spherical shape of the Earth. The Mercator projection increases the difference of transformed latitude to exactly reach the same difference of longitude (measured in degrees). The Mercator projection is not defined at the poles, however the South Pole is located on land, and the Arctic region north of 85N is not included in our study.

Longitude and latitude become isotropic with the Mercator projection, and the radius of effect (in meter) of each measurement point will decrease as $\sin(\varphi)$. Thus, this will also take into account the decrease of the Rossby radius of deformation
115 with latitude.

The distance to every measurement point is computed around each grid point:

$$d_i^2 = \left[\frac{\Delta\lambda}{L_\lambda}\right]^2 - \left[\frac{\Delta\varphi'}{L_{\varphi'}}\right]^2 - \left[\frac{\Delta t}{L_t}\right]^2 \quad (6)$$

with $\Delta\lambda$ the difference of longitude between the grid point and the measurement point (modulo 360, accounting thus for
120 periodic condition), $\Delta\varphi'$ the difference of Mercator latitude, and Δt the number of days of difference (modulo 365.25 if producing the climatology). The three L express the decorrelation scales for longitude, Mercator latitude and time. The three decorrelation scales have been chosen as: $L_\lambda = L_{\varphi'} = 3.3^\circ$, and $L_t = 45 \text{ d}$, similar to the coefficient used to produce the MIMOC climatology (Schmidt et al., 2013).

The 300 closest points are selected for the RBF interpolation. If less than 50 points are located in a sphere with distance $d = 1$
125 around the grid point, the grid point is masked and no interpolation is done (distance of 1 corresponds to e.g. $\Delta\lambda = L_\lambda$ or $\Delta t = L_t$). While this is not a big issue for the climatology, we acknowledge that it filters out some of grid point in e.g. the Southern Ocean or Arctic Ocean. However, it seems honest to mask grid points with not enough observation in its neighbourhood. The

choice of 50 points is somehow arbitrary, more work should be needed to provide an estimate of the minimum number of profiles needed.

130 The interpolation kernel uses a Gaussian function, the weighting function is:

$$w_i = \exp(-d_i^2 \epsilon^2) \quad (7)$$

ϵ is a shape parameter that changes whether the gaussian is flat or spiked. A large ϵ produces a spiky interpolation, as only the very close points will have a non-negligible distance. On the opposite, a small ϵ leads to a very smooth field. $\epsilon = 0.5$ is chosen as a good fit between smoothing and not only keeping the very large scale.

135 The covariance matrix between all the measurement points is defined as:

$$E_{ij}^0 = \exp(-d_{ij}^2 \epsilon^2) \quad (8)$$

using the distance between all points. A constant noise-signal ratio is added to \mathbf{E}^0 , i.e. $\mathbf{E} = \mathbf{E}^0 + \lambda \mathbf{I}$.

The interpolation at a point x is given by

$$s(x) = \Phi(x) \cdot \omega \quad (9)$$

140 where $\Phi_i(x) = \exp(-d_{xi}^2 \epsilon^2)$, and ω is the solution of

$$\mathbf{E} \cdot \omega = \Psi \quad (10)$$

with Ψ the vector of measured properties. The final formula is then:

$$s(x) = \Phi \cdot \mathbf{E}^{-1} \cdot \Psi \quad (11)$$

By using either the time in Julian days, or in days of year, it is possible to use the same method to produce climatological fields or the monthly field of a certain year. While the interpolation method allows estimating variance (and thus error) associated with the computation, it highly depends on *a priori* estimates of the variance of the measures, which value is not known. Instead, we compute monthly products for years 2004 – 2021, and estimate the monthly standard deviation of MLD and SCI at each point, using the 17 years of the product. Due to the criteria of using strictly more than 50 points close by, some data points are not used for the monthly product, but only used in the climatology.

150 A regular longitude – latitude grid with a resolution of 1 degree is used for the mapping to produce monthly products.

During the interpolation, grid points are masked if they have less than 50 points in a circle of radius 1. Fortunately, this threshold does not affect the major part of the ocean, except for polar regions, especially the Arctic Ocean (Fig. 2). Some hotspots of measurement are visible, e.g. the Kerguelen Plateau (69E, 49S), in the Southern Ocean where seals are tagged with CTD sensors.

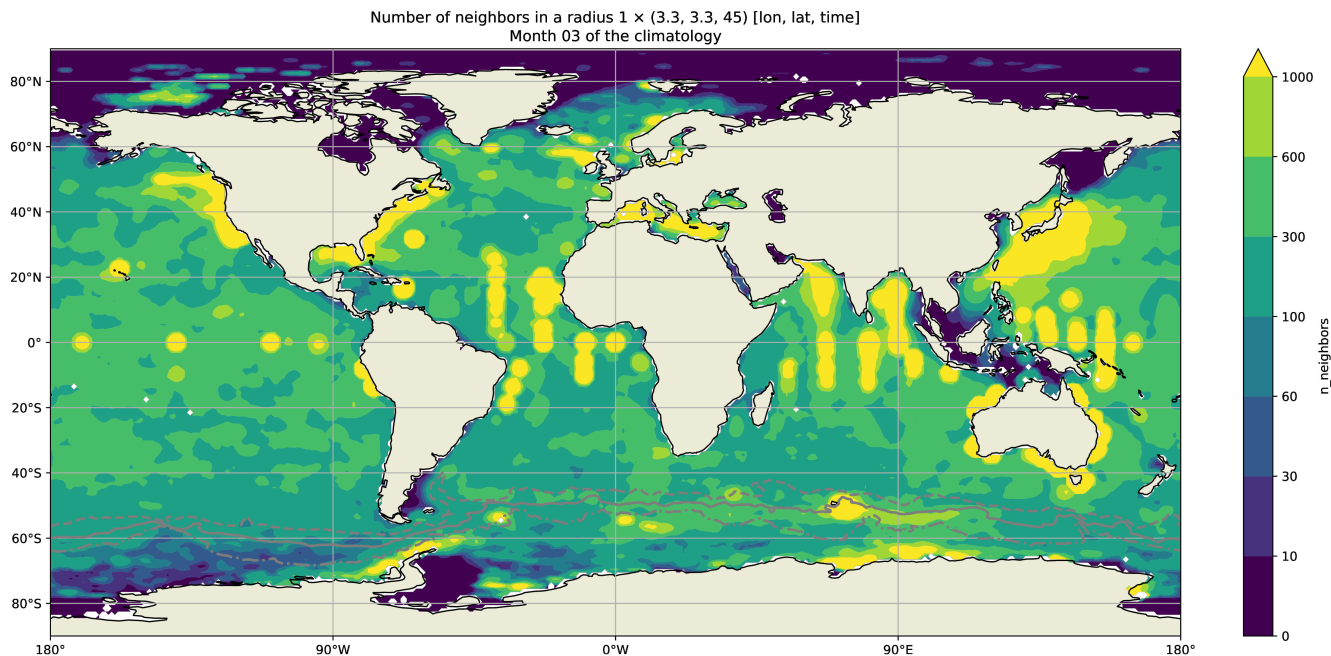


Figure 2. Number of profiles in a circle of distance 1 of each grid point for the month March. All years are taken into account. The distance is measured by Eq. (6) and is unitless.

155 3 Results

3.1 MLD climatology

In winter, the MLD is deep only in a few regions: the Labrador Sea, the Irminger and Nordic Seas, along the coast of Antarctica and in the Deep Mixing Band (DMB) north of the ACC (Fig. 3). These regions are also the regions where the climatological state is not precise due to large interannual variations (Fig. 4). In the North Pacific Ocean, a maximum of MLD is found around 40N. This is the location of the transition between subtropical and subpolar water (Roden, 1970). The SO DMB is present north of the SAF, and other regions in the SO exhibit ML deeper than their neighbourhood. Such a slightly deeper pool is visible south of the Kerguelen Islands. A narrow band of MLD of about 200 m is present in the South Atlantic Ocean, north of the ACC.

Deep winter mixed layers are found just north of the SAF in the DMB, ranging from 200 to 400 m (Fig. ??) (Dong et al., 2007; DuVivier et al., 2018). Some deep ML regions are contained within the PFZ, south of New Zealand around 175E, 57S, and in the south-east Pacific basin where some PFZ pools MLD can exceed 200 m. The mixed layer is overall shallower in the Atlantic basin in the SAF compared with the Indian and Pacific basins. From 180E to 210E in the SAZ, the ML are getting shallower, before deepening again and be deeper than 300 m before the Drake Passage. Within the PFZ, the mixed layer is

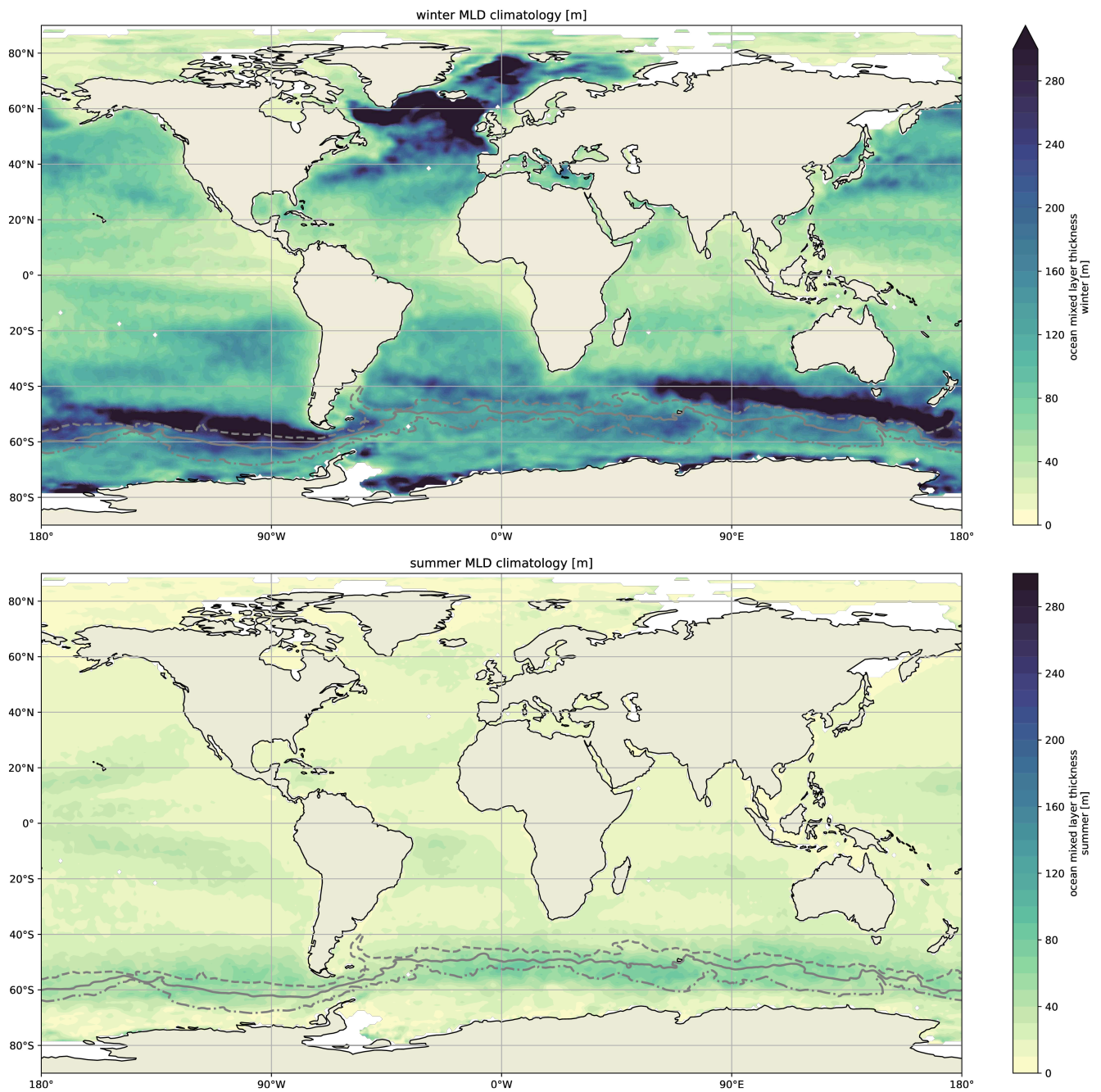


Figure 3. Climatologies of winter (deepest) and summer (shallowest) MLD. In the SO, the 3 gray lines represent from north to south the SAF, the PF, and the SACCF.

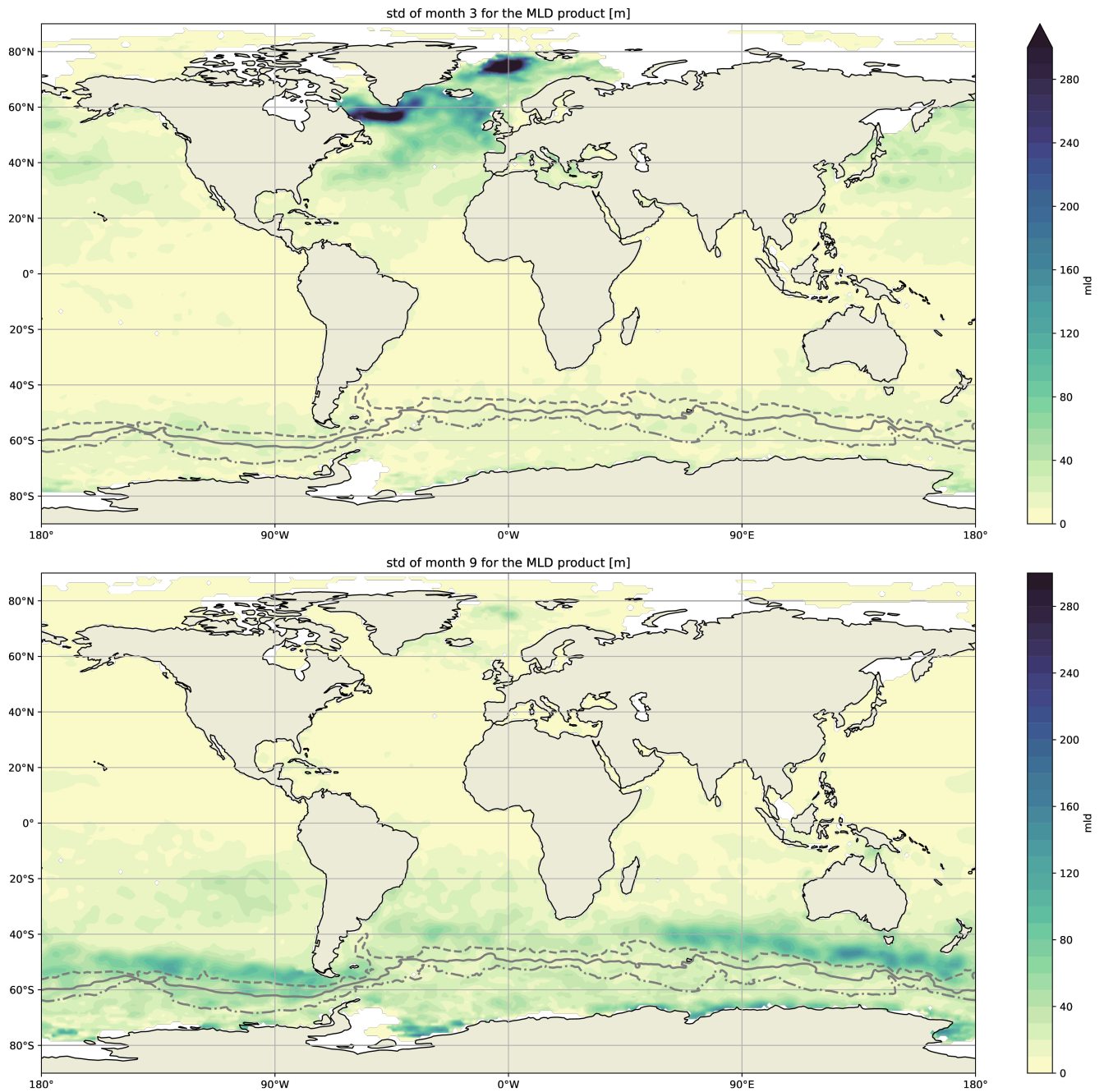


Figure 4. Standard deviation of monthly MLD for 2004 – 2021 period in March and September.

overall shallower, and is about 150 m deep. Apart from the major deep pool within the PFZ, some regions have slightly deeper
170 MLs, e.g. south of the Kerguelen islands in the Indian Ocean, and north of the SAACF at about 90E.

In summer, the deepest ML worldwide are found within the ACC. The centre of the subtropical gyres have ML of about
20-30 m while being less than 10 m at their borders.

In summer, the ML is shallower everywhere. A major difference with the winter one, is that the ACC region presents the
deepest ML, that are about 60 m deep, while the SAZ and SACCZ MLs are about 25 m deep.

175 In winter (March in the Northern Hemisphere, September in the Southern Hemisphere), the largest interannual variability
occurs in regions of deep ML. In the North Atlantic, large interannual variability exists in the Labrador Sea, the Irminger Sea,
and the Nordic Seas. However, scaling the standard deviation by the average presents a more uniform picture. The standard
deviation is equal to about half of the mean MLD (Fig. B1 in Appendix). These regions of large interannual variability in the
MLD are intrinsically misrepresented in a climatological state.

180 The DMB in the SO, with winter MLs on average deeper than 250 m, also exhibits interannual variability. The SO is overall
poorly sampled due to its remote location, and part of the interannual variability that we see could arise from a sampling of
water masses not representatives of the surrounding neighbourhood. To highlight the interannual variability, we compare our
monthly product with time series of MLD from each profile at a distance 1 from the point (85.5E, 42.5S), located in the DMB
north of the Kerguelen Plateau (Fig. 5). The median MLD in this circle is deeper than 500 m in the winter of 2014, and is 230 m
185 in the winter of 2017. These 2 winters are the 2 extrema present in the time series, and both correspond to months with a fair
amount of data. In months with little or no data (e.g. winter 2005 or summer 2008), the monthly product is computed using
points located at a greater distance, which explains why in winter 2005 our product shows a maximum ML of 250 m while
the median peaks at 450 m. The monthly climatology uses all points available for every year and thus smoothes the extreme
events. Plotting all the MLD measurements as function of day of year allows for a direct comparison with the climatology
190 (Fig. 5). Our climatology is in good agreement with the individual points, with a maximum MLD of almost 400 m in August
and September.

The Irminger Sea in the North Atlantic Ocean is one of the places where deep convection occurs in winter. Deep convection
does not occur every year (Fig. 6). The winter 2014-2015 presents strong convection with MLD reaching 1000 m. Opposite,
the MLD can be as shallow as 200 m in other winters. On a climatological state, the MLD follows a strong seasonal cycle, with
195 winter MLD of about 400 m and summer MLD of 40 m (Fig. 6(d)).

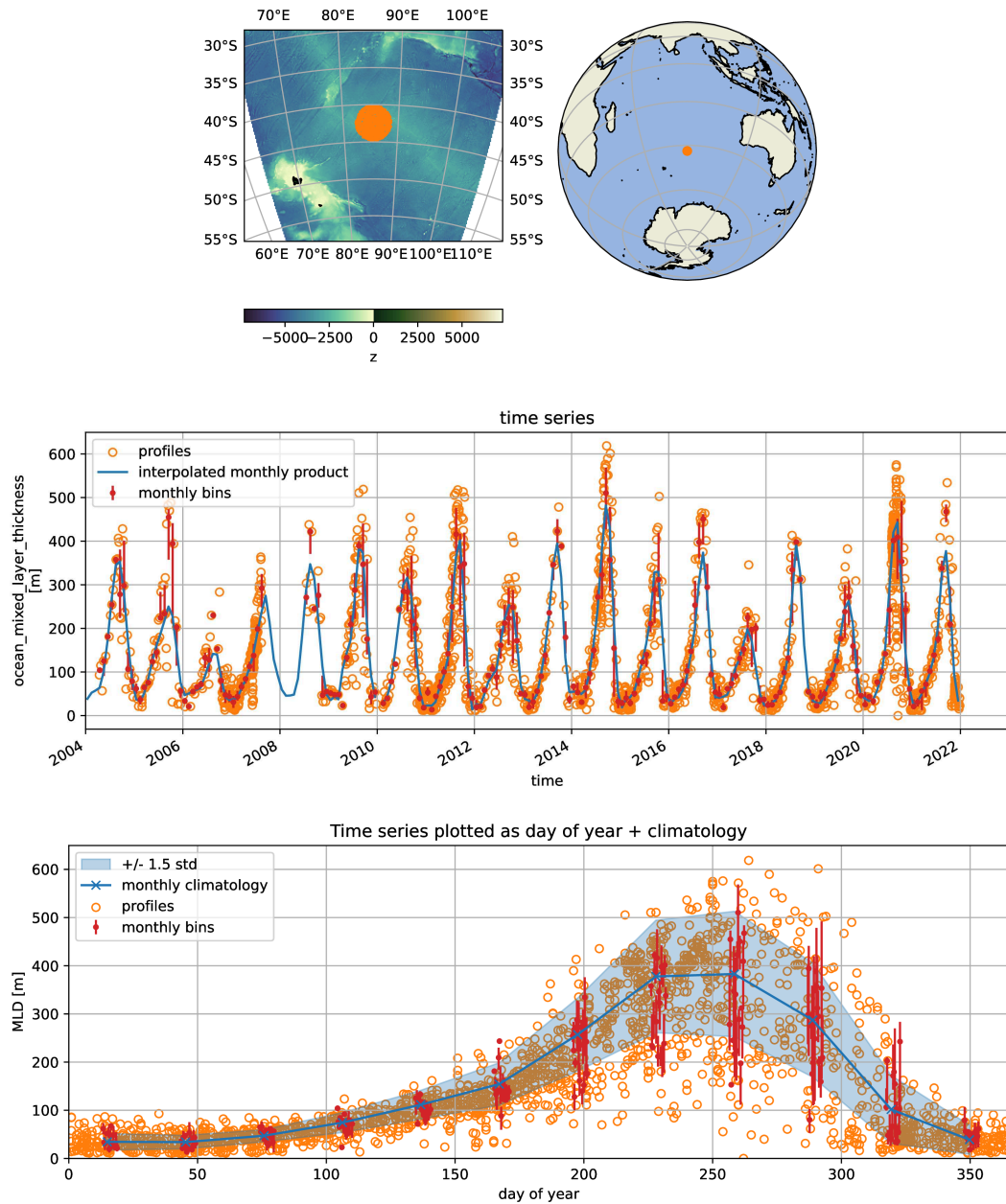


Figure 5. Time series of the MLD north of the Kerguelen Plateau, in the deep mixing band of the SO. The bathymetry and location of the profiles are shown in the upper row, the middle row presents the time series of the profiles MLD, the median and quartiles of monthly binned profiles, and our monthly interpolated product. The ticks and vertical lines are plotted the 1st of January of the years. The bottom row present our monthly climatology. All profiles in a distance 1 of the point (85.5E, 42.5S) are used.

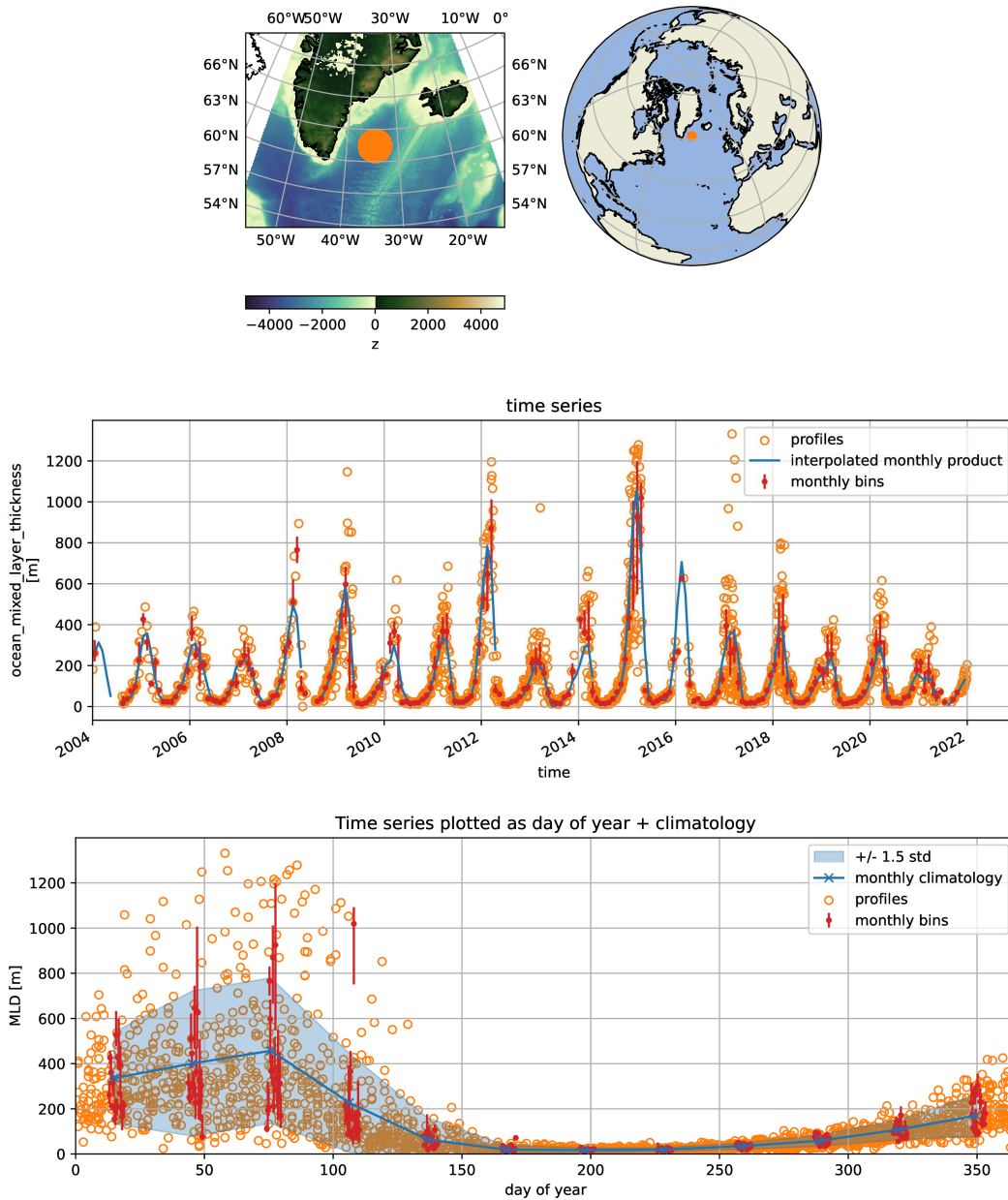


Figure 6. Time series of the MLD in the Irminger Sea. The bathymetry and location of the profiles are shown in the upper row, the middle row presents the time series of the profiles MLD, the median and quartiles of monthly binned profiles, and our monthly interpolated product. The ticks and vertical lines are plotted the 1st of January of the years. The bottom row present our monthly climatology. All profiles in a distance 1 of the point (325.5E, 61.5) are used.

3.2 SCI climatology

The SCI computed below the ML gives information on the stratifying agent. For $SCI > -1$ temperature decreases with depth and thus increases stratification, and for $SCI < 1$ salinity increases with depth, also increasing stratification. In winter, the majority of the ocean equatorward of the polar regions is classified as alpha ocean ($SCI > 1$) for mid-latitudes, and transition zone ($-1 < SCI < 1$) for tropical regions (Figs. 7 and 8). Evaporation is larger than precipitation in the subtropical gyres, so the surface salinity is larger than below the ML. Opposite, due to the large freshwater input from rain at the equator, the surface salinity is low and thus salinity stratifies in the tropical regions.

Beta ocean ($SCI < -1$) is found in the polar regions, south of 50-60S in the SO and north of 40-50N in the Pacific Ocean. In the North Atlantic Ocean, the alpha – beta separation does not follow a zonal pattern. Alpha ocean is present in the eastern part of the Atlantic Ocean north of 40N, and beta ocean is found in the western part. Using an idealised basin configuration of a numerical ocean model, Caneill et al. (2022) found a similar diagonal orientation of the transition zone. The southward advection by the subpolar gyre on the western part of the basin brings cold and fresh surface water, which creates the tongue of beta ocean along the coast of America.

The transition zone between subtropical (alpha) and polar (beta) water is generally narrow, except in the north-east Pacific Ocean, where the transition zone is 20 degrees of latitude wide (Figs. 7 and 8).

In the tropical ocean, the summer SCI is close to the winter SCI, where the MLD does not follow a strong annual cycle. The centre of the subtropical gyres are classified as alpha ocean in summer, but the SCI is smaller than in winter, indicating that salinity has a smaller destratifying effect in summer. The largest differences in SCI between summer and winter happen poleward of 40N or 40S. In summer, poleward of 40 degrees, the ocean is classified as transition zone. Indeed, the summer heat fluxes warm the upper layer of the ocean, thus temperature decreases with depth even in the polar regions. The SCI stays negative in the polar regions, indicating that despite relative warm water in the mixed layer, salinity remains the main stratifying agent. As pointed out by Roquet et al. (2022), the thermal expansion coefficient is small in cold water, reducing the impact of temperature on stratification. In summer, water in polar regions remains cold, so only very large gradients of temperature produce a similar stratification as the salinity gradient.

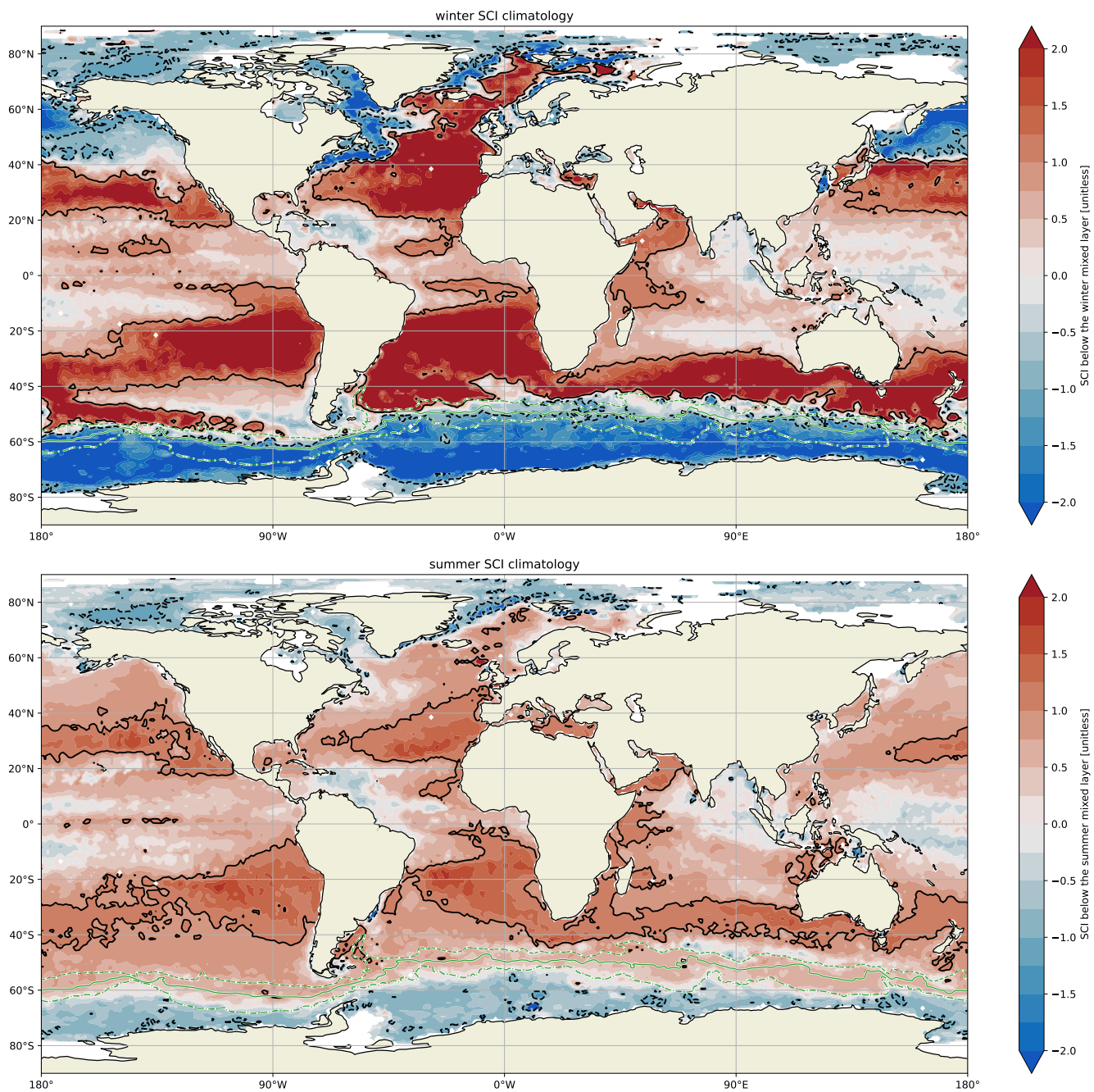


Figure 7. Climatologies of the SCI below the winter and summer ML. The white and green lines in the SO represent the 3 majors fronts of the ACC. The continuous black line is $SCI = 1$, the dashed black line is $SCI = -1$.

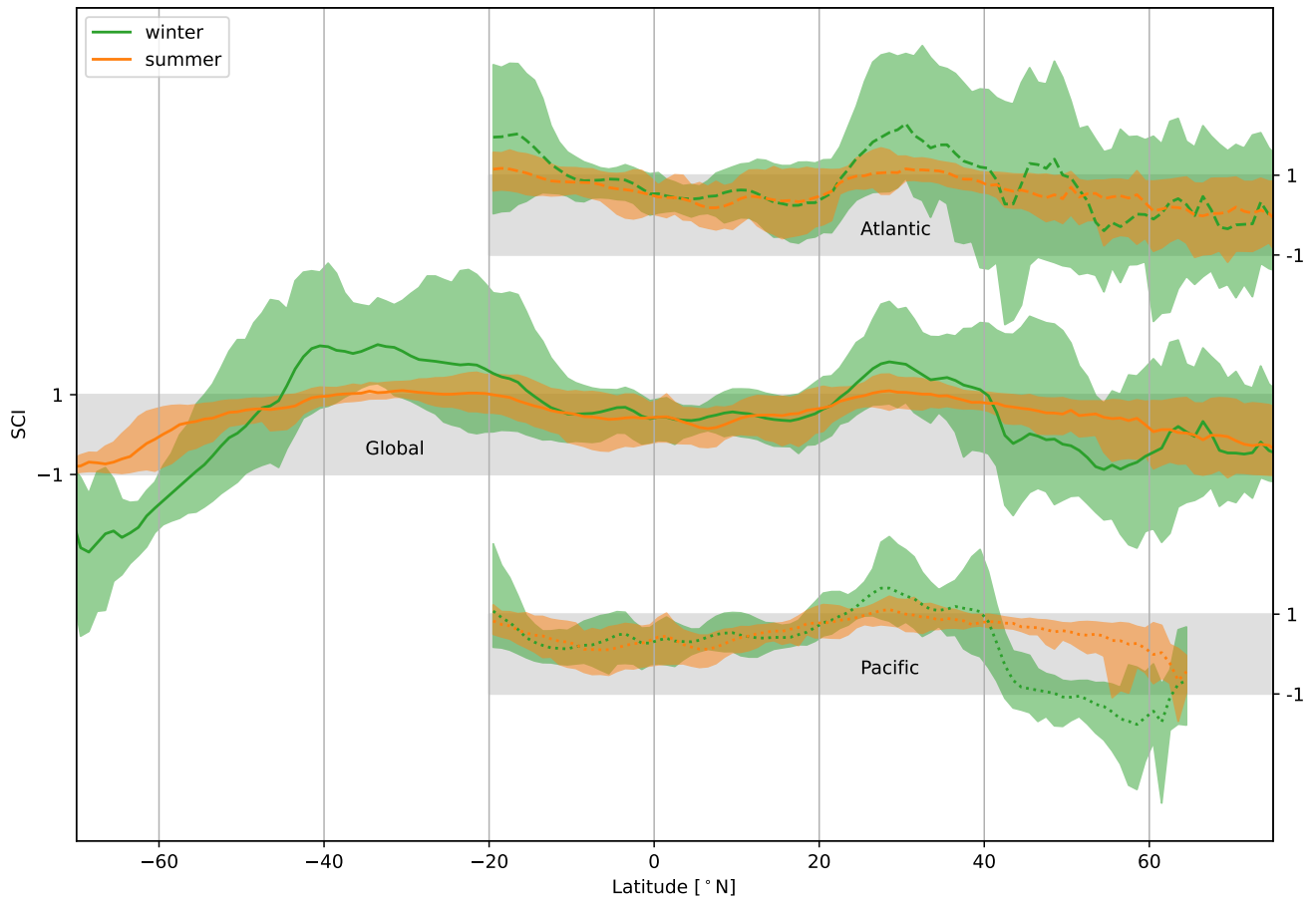


Figure 8. Zonal climatology of winter (green) and summer (orange) SCI below the mixed layer. The lines are the zonal means, and the shadings are the 10th and 90th percentiles. The middle lines are the global zonal means. The upper and lower lines, starting at 20°S, separate the Pacific basin, where the SCI is approximately zonally constant, from the Atlantic basin, where the SCI encounters large longitudinal variations. The Atlantic and Pacific zonal means have been shifted vertically for clarity, and they refer to their own axis on the right. The gray bands represent $-1 < SCI < 1$.

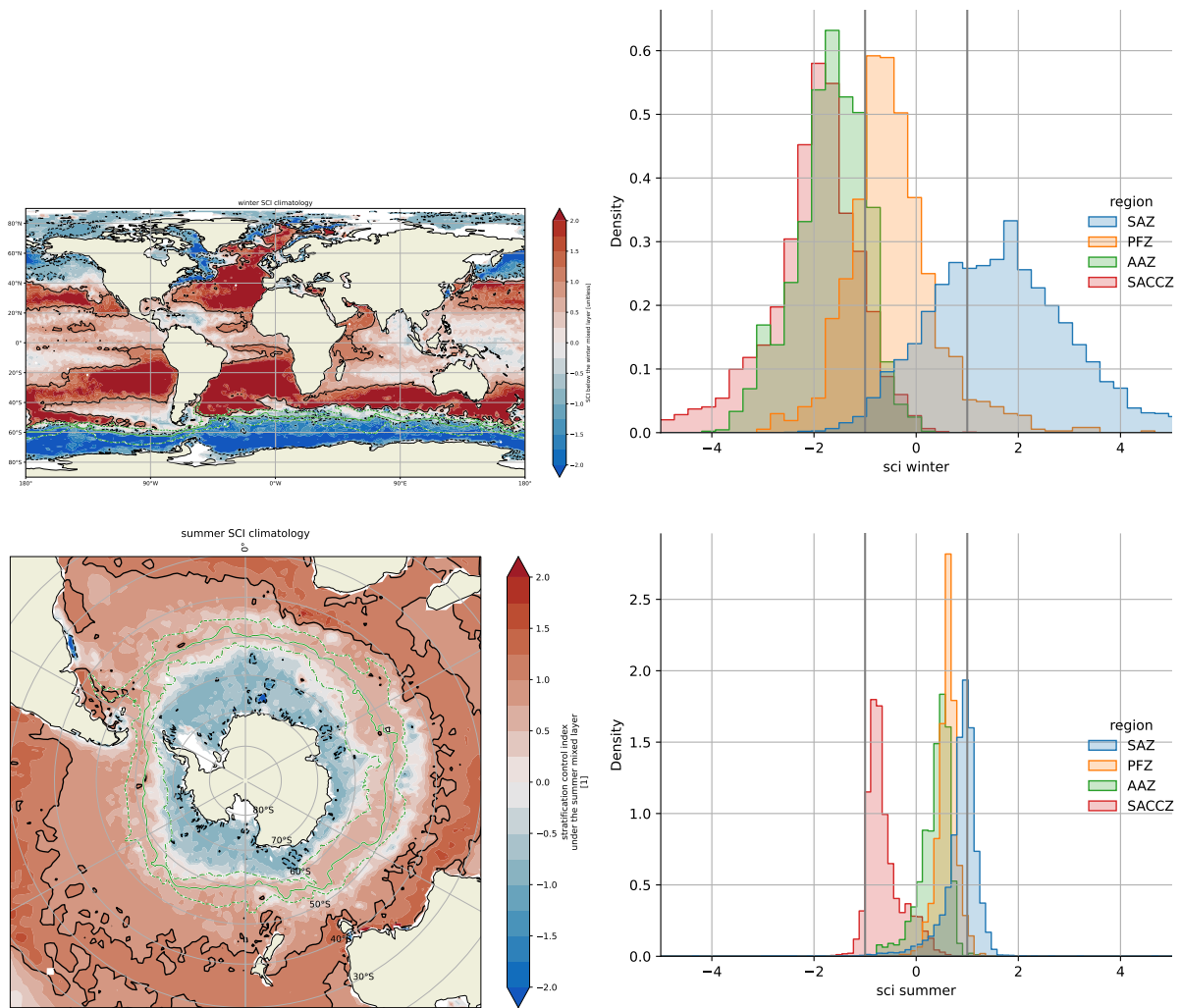


Figure 9. Climatology of the winter / summer SCI (left column), and histograms of the SCI per zone of the SO (right column).

220 In the Southern Ocean, there is an interesting connection between the SCI and the main frontal features. The position of winter $SCI = 1$ is located close to the SAF (Fig. 9). This is expected if we follow the Pollard et al. (2002) definition of the SAF as being the southern boundary of the region stratified by temperature and destabilized by salt. However, the $SCI = 1$ front is not a simple circumpolar closed line that monotonically turns around Antarctica. In the south-east Pacific, the $SCI = 1$ contour shifts westward and surrounds a transition zone tongue that seems to emanate from South-America. This layer is the

225 surface expression of the Shallow Salinity Minimum Layer (SSMW), also called Eastern South Pacific Intermediate Water (Karstensen, 2004). The SSMW is a layer of minimum salinity, outcropping at about 45S in the south-east Pacific Ocean, and then subducting to about 200 m. It is a minimum salinity because of the combination of Ekman transport of freshwater

precipitation, and a slow geostrophic velocity within the ML, creating a freshwater flux larger than the area surrounding it when integrated temporally (Karstensen, 2004). The SSMW is fresher than the AAIW that lies below it, and hence the region
230 where SSMW surfaces must have $SCI > -1$.

Two main transition zones tongues interlocking into alpha region are found: one in the Atlantic basin centred around (0E, 40S), and the other south of New-Zealand (around 175E, 47S). A difference between these 2 tongues is the sign of the SCI: the Atlantic one has $SCI > 0$, so salinity contributes less than temperature to stratification, while the New-Zealand's one has $SCI < 0$, so is mainly stratified by salt. The New-Zealand transition tongue is also associated with a ML shallower than the
235 surrounding ocean, while the Atlantic Ocean one is not marked by a change of MLD. The mean dynamic topography (MDT) gives information on the mean surface geostrophic flow. Close to New-Zealand, there is a meander going northward and then back southward. This meander could bring slightly colder and fresher water in this region. The MDT gradient is smaller in this region, implying smaller geostrophic flow, and hence more time for water to gain freshwater from the precipitation, creating a surface layer fresher than the layer below.

240 In summer, temperature is the most important component of stratification ($SCI > 0$), except in SACCZ where $-1 < SCI < 0$. A small region of the SAZ in the Indian Ocean also has $SCI > 0$.

3.3 Seasonality of the SCI

Using a gridded ARGO product, DuVivier et al. (2018) computed the type of stratification below the ML in the DMB of the SO. They found that the stratification follows a strong seasonality, moving from transition zone in spring, to beta ocean in some area
245 in June, and finally alpha ocean in winter. The MLD reaches this salinity maximum, when $SCI < 1$ in the time series around the (85.5E, 42.5S) point (Fig. 10). Above the salinity maximum, as salinity contributes to increasing stratification, $SCI < 1$. When the ML passes below it, salinity decreases with depth and $SCI > 1$. The ML reaches below the salinity maximum in July, when SCI becomes larger than 1. The climatological MLD in July is 250 m in this point (Fig. 5), so below 250 m salinity decreases with depth and the ocean is classified as alpha. In June, $SCI < -1$ which indicates a temperature inversion in the
250 water column, at a depth of 150 m (Fig. 5).

South of the PF, salinity is the stratifying agent and temperature destratifies below the winter ML. Around the point (65.5E, 53.5S) located to the west of the Kerguelen Plateau, the SCI is below 1 all year long for the majority of the profiles (Fig. 11). This indicates that salinity always increases with depth below the ML. $SCI < -1$ in August, September, and October when the ML is the deepest and has eroded the summer stratification. The winter temperature of the ML is colder than the water
255 below, the defining feature of beta ocean.

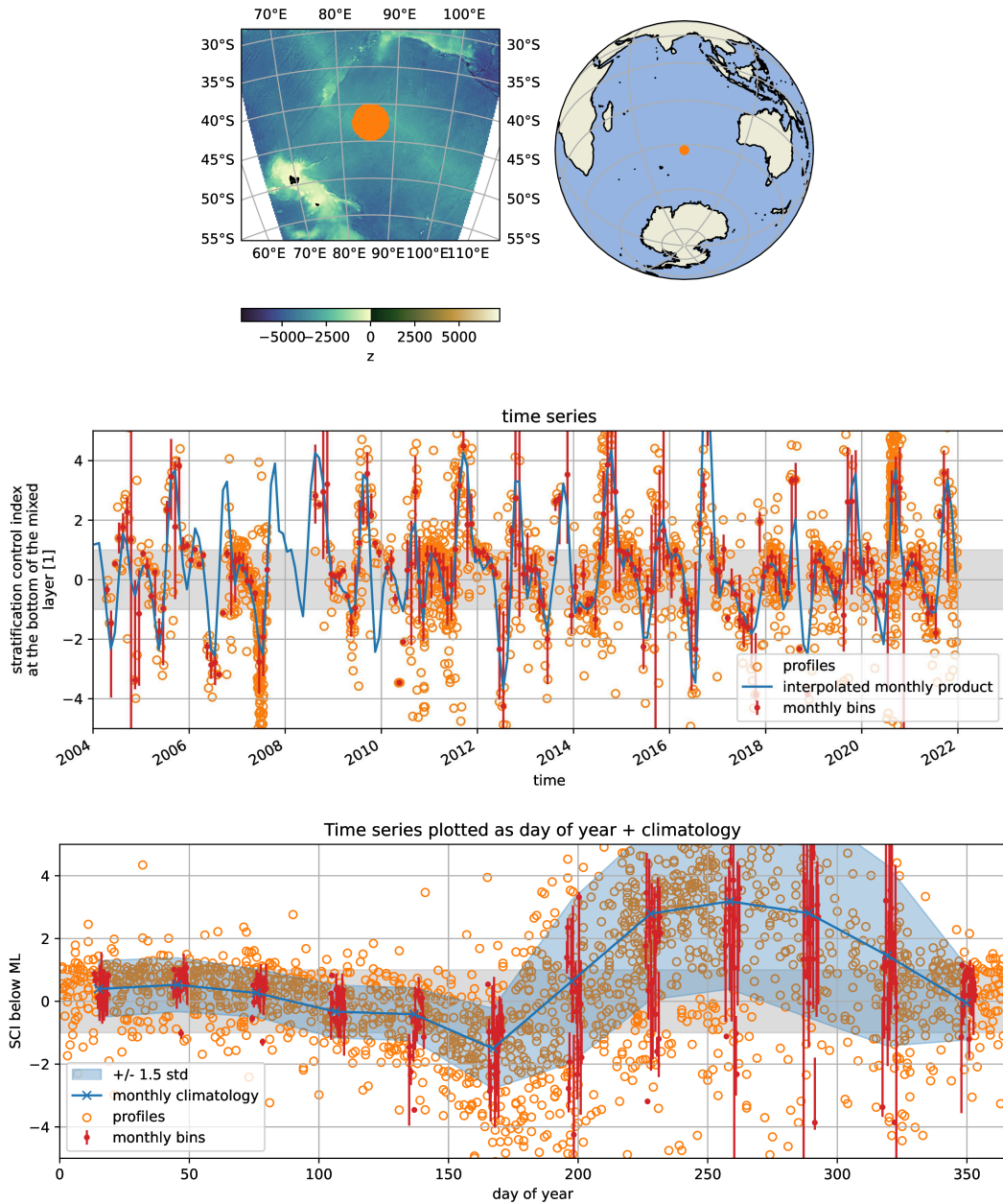


Figure 10. Time series of the SCI in the DMB, north of the Kerguelen Plateau. The location in alpha ocean in winter.

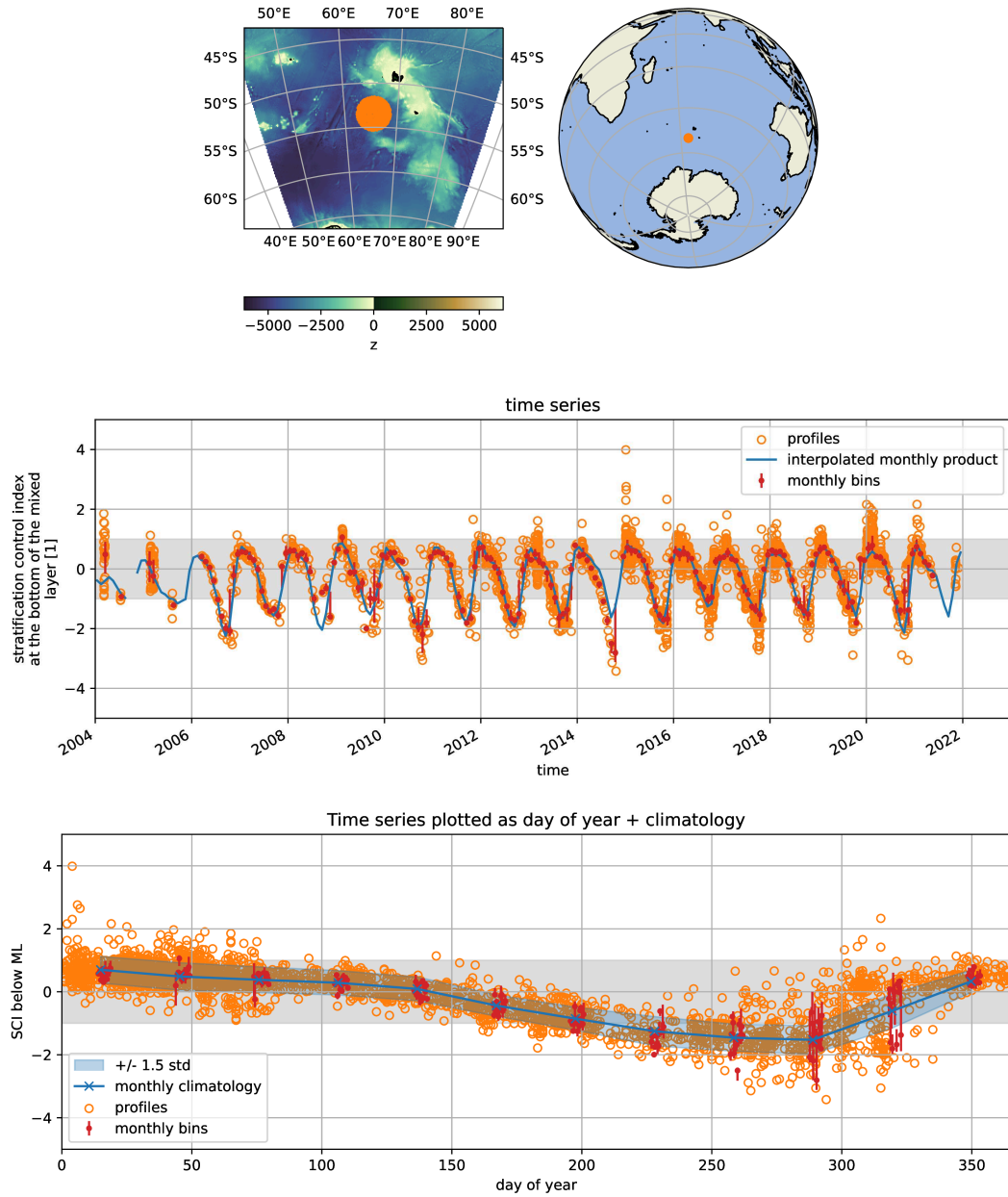


Figure 11. Time series of the SCI south-west of the Kerguelen Plateau. The location is in beta ocean in winter.

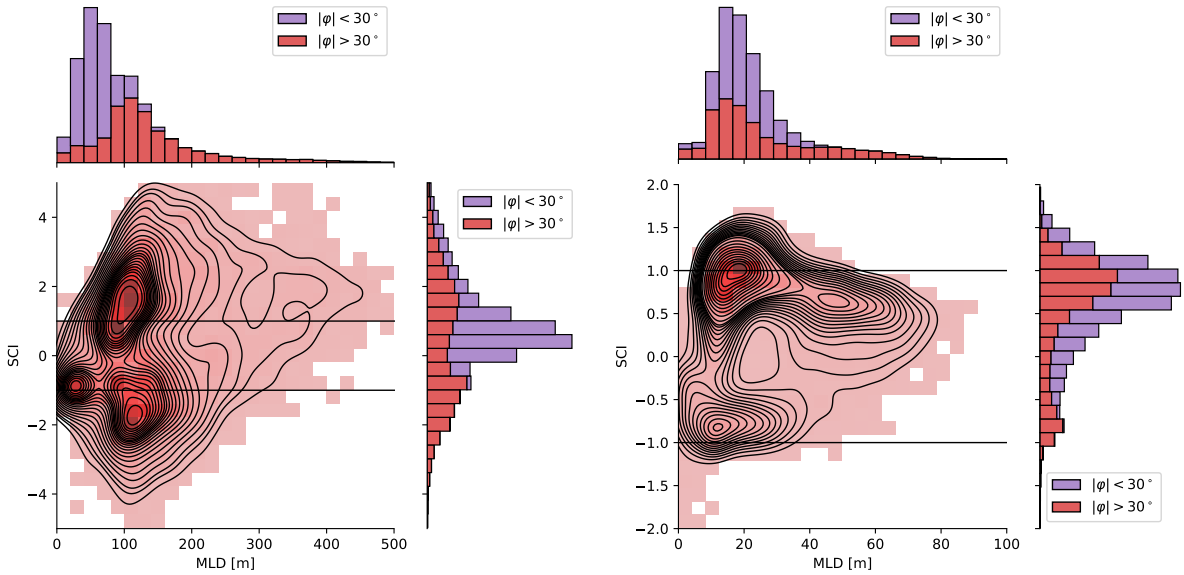


Figure 12. SCI versus MLD in winter (left) and summer (right). The centre figures represent a 2 dimensions histogram (colours), with a kernel density estimation (contour lines) superimposed. For the centre figures, only data with a latitude $|\varphi| > 30^\circ$ are shown. The histograms on the sides are split into the tropical regions ($|\varphi| < 30^\circ$) in purple, and the rest of the ocean ($|\varphi| > 30^\circ$) in red. The upper histograms are for the MLD, and the histograms on the right are for the SCI. Data are taken from the 1° climatologies. Each data point is weighted by the area of its corresponding cell of the 1° grid.

3.4 On the link between the SCI and the MLD

Deep MLs occur more often in alpha oceans than in beta oceans or transition zones (Figs. 3 and 7). plotting the SCI versus the MLD (Fig. 12). MLs deeper than 250 m are mostly found in the alpha oceans (larger values of the two-dimensional histogram, Fig. 12). Deep MLs are also found in oceans classified as transition zones and are almost absent in beta oceans. Individual profiles in the beta oceans show deep MLs along the coast of Antarctica, but they represent a small area and are thus not seen in this figure.

Tropical regions (defined here with an absolute value of the latitude less than 30°) are only plotted on the top and right histograms. They represent a large area with shallow MLs (less than 100 m) and are classified almost exclusively as transition zones.

For higher latitudes ($|\varphi| \geq 30^\circ$), the ML distribution exhibits a peak at 120 m. The SCI distribution poleward of 30° is bimodal, centred around ± 1.5 . The oceans thus encounter partial compensation between temperature and salinity more often than when temperature and salinity both stabilise. Poleward of 30° , the shallowest MLs are found in regions where salinity dominates the stratification ($SCI < 0$), either in transition zones or beta oceans. Regions that encounter large density compensation (large $|SCI|$) do not present shallow ML.

270 In summer, MLs are shallow and the SCI is bimodal, both in tropical oceans and at higher latitudes. The majority of the ocean has a SCI around 1, representative of the summer thermocline. The majority of the oceans is located in a peak of $MLD = 20$ m and $SCI = 1$.

4 Discussion and conclusions

275 In this work we computed monthly climatologies and monthly products for the years 2004 – 2021, for the mixed layer depth, and stratification control index below the ML, based on the EN4.2.2 profiles. After computing the MLD and SCI on individual profiles, we used a radial basis function interpolation to create the monthly products and climatologies. Despite its simple structure in two dimension, the SCI below the winter ML provide a comprehensive overview of the large scale oceanic circulation and main feature, as well as the regional discrepancies.

280 Region of deep and intermediate water formation are visible on the climatological state of the winter MLD (Fig. 3). In the Northern Hemisphere, MLs are deeper in the Atlantic Ocean than in the Pacific Ocean, the signature of the absence of deep water formation in the North Pacific. In the Atlantic Ocean, ML are deepest in the Labrador, Greenland, Island, and Norwegian Seas. The signature of the Gulf Stream and the Kuroshio Current can be followed by looking at the local maxima of MLD around 40N. In the SO, ML are deepest in the deep mixing band located north of the ACC, and close to the coast of Antarctica where deep water is formed in winter in coastal polynyas.

285 The regions of deepest MLD also present large interannual variability (Fig. 4). On average, the standard deviation of the MLD along years, for every month, is half of the climatological value. Part of this variation is certainly representative of the intrinsic interannual variability of the ocean, part could also come from spatial variability and unrepresentative sampling.

290 Time series of profiles from the DMB and Irminger Sea, two regions with deep ML in winter, both present large variability between years, and between profiles at the same date. In the Irminger Sea, convection occurs occasionally and was weak in the early 2000s before being more active in years 2015 – 2018 (Sterl and De Jong, 2022). Whether the climatological state should represent the years with or without convection may depend on the research question. In energetic regions, the mean state differs from snapshots states at meso- and submeso-scales. With a limited amount of observations, errors associated with individual profiles compared to mean state can be large. Future work needs to be done to assess the minimum number of profiles necessary to compute a representative mean state of a region.

295 As noted by Carmack (2007), polar regions are stratified by salinity, and subtropical to subpolar regions are stratified by temperature. The winter climatology of the SCI emphasizes this separation (Fig. 7). Alpha ocean reaches far north in the eastern side of the Atlantic Ocean, where MLD is deep in winter. In the Labrador Sea where MLD is also deep in winter, the ocean is classified as beta or transition zone. In the SO, the DMB is located in alpha ocean, except in the eastern Pacific Ocean where it is transition zone. Deep convection site close to Antarctica are located in beta ocean. Freshwater input at the surface of the ocean helps to build the polar halocline. Fluxes alone do not explain the alpha – beta distinction, cold water density variation is almost not sensitive to variation in temperature, so the strong winter heat loss is not able to destabilise the water column and the temperature inversion is maintained (Caneill et al., 2022; Roquet et al., 2022).

The main fronts of the ACC can be linked to the type of stratification (Pollard et al., 2002; Pauthenet et al., 2017). While in the Atlantic and Indian Oceans, the SAF and PF are closely related to the position of the winter $SCI = \pm 1$, in the eastern Pacific Ocean the SAF is located in the transition zone. The vision of dynamical fronts as circumpolar features is not representative of the reality, as jets are usually transient and a contour of SSH associated with a large SSH gradient at a time can correspond to a flat area somewhere else (Chapman et al., 2020). The meridional change of stratification is however a circumpolar feature, but cannot be directly linked to dynamical fronts.

MLD is commonly used to validate or compare climate models (e.g. Treguier et al., 2023). The SCI is a quantity easy to compute, but that still provides at a glance a global overview of the ocean state. Future work could be conducted to compare the SCI in ocean models with our newly produced climatology.

In conclusion, we computed new climatologies of MLD and SCI. The maps of the winter SCI provide an overview of the global ocean stratification. Polar regions appear to be the only places stratified by only salinity (beta ocean), as remarked by Carmack (2007) in precise locations. In the North Atlantic, the beta ocean goes down along the coast of America down to 40N, while the alpha ocean goes up to 80N on the eastern side of the Nordic Seas. In contrast, the transition between alpha and beta oceans is fairly zonal and centred around 40N in the North Pacific Ocean. The different zones of the SO defined by Pollard et al. (2002) stand out in the SCI maps. This study provides a global description of the ocean state.

Code and data availability. The code and data will be available upon acceptance of the manuscript.

Appendix A: Comparison of raw and smoothed temperature profile

Appendix B: MLD mean and standard deviation

Author contributions. TEXT

Competing interests. TEXT

Disclaimer. TEXT

Acknowledgements. TEXT



Figure A1. Comparison of raw and smoothed temperature profile.

325 References

- Caneill, R., Roquet, F., Madec, G., and Nycander, J.: The Polar Transition from Alpha to Beta Regions Set by a Surface Buoyancy Flux Inversion, *Journal of Physical Oceanography*, 52, 1887–1902, <https://doi.org/10.1175/JPO-D-21-0295.1>, 2022.
- Caneill, R., Roquet, F., and Nycander, J.: Southern Ocean deep mixing band emerges from a competition between winter buoyancy loss and upper stratification strength, *EGUsphere*, 2023, 1–29, <https://doi.org/10.5194/egusphere-2023-2404>, 2023.
- 330 Carmack, E. C.: The alpha/beta ocean distinction: A perspective on freshwater fluxes, convection, nutrients and productivity in high-latitude seas, *Deep Sea Research Part II: Topical Studies in Oceanography*, 54, 2578–2598, <https://doi.org/10.1016/j.dsr2.2007.08.018>, 2007.
- CCHDO Hydrographic Data Office: CCHDO Hydrographic Data Archive, Version 2023-11-21, <https://doi.org/10.6075/J0CCHAM8>, in CCHDO Hydrographic Data Archive, 2023.
- Chapman, C. C., Lea, M.-A., Meyer, A., Sallée, J.-B., and Hindell, M.: Defining Southern Ocean fronts and their influence on biological and physical processes in a changing climate, *Nature Climate Change*, 10, 209–219, <https://doi.org/10.1038/s41558-020-0705-4>, 2020.
- 335 Clément, L., McDonagh, E. L., Marzocchi, A., and Nurser, A. J. G.: Signature of Ocean Warming at the Mixed Layer Base, *Geophysical Research Letters*, 47, <https://doi.org/10.1029/2019GL086269>, 2020.
- Curry, J. A., Schramm, J. L., and Ebert, E. E.: Sea Ice-Albedo Climate Feedback Mechanism, *Journal of Climate*, 8, 240–247, [https://doi.org/10.1175/1520-0442\(1995\)008<0240:SIACFM>2.0.CO;2](https://doi.org/10.1175/1520-0442(1995)008<0240:SIACFM>2.0.CO;2), 1995.

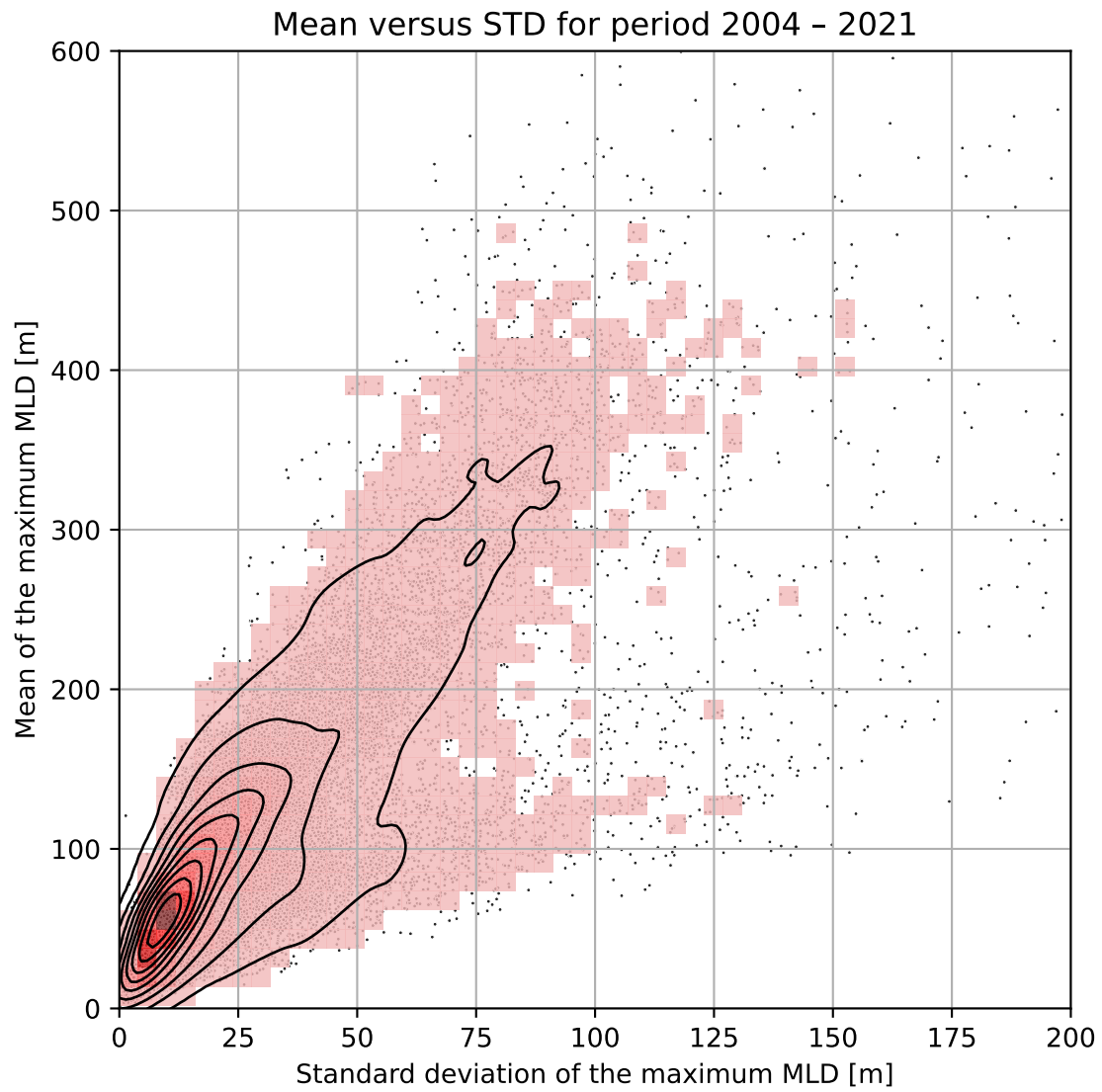


Figure B1. Mean of the MLD versus the standard deviation (for winter). The means are taken along years of the monthly product.

- 340 de Boyer Montégut, C.: Mixed layer depth over the global ocean: An examination of profile data and a profile-based climatology, *Journal of Geophysical Research*, 109, C12 003, <https://doi.org/10.1029/2004JC002378>, 2004.
- de Boyer Montégut, C.: Mixed layer depth climatology computed with a density threshold criterion of 0.03kg/m³ from 10 m depth value, <https://doi.org/10.17882/91774>, 2023.
- Dong, S., Gille, S. T., and Sprintall, J.: An Assessment of the Southern Ocean Mixed Layer Heat Budget, *Journal of Climate*, 20, 4425–4442, 345 <https://doi.org/10.1175/JCLI4259.1>, 2007.
- DuVivier, A. K., Large, W. G., and Small, R. J.: Argo Observations of the Deep Mixing Band in the Southern Ocean: A Salinity Modeling Challenge, *Journal of Geophysical Research: Oceans*, 123, 7599–7617, <https://doi.org/10.1029/2018JC014275>, 2018.
- Emery, W. J.: Antarctic Polar Frontal Zone from Australia to the Drake Passage, *Journal of Physical Oceanography*, 7, 811–822, [https://doi.org/10.1175/1520-0485\(1977\)007<0811:APFZFA>2.0.CO;2](https://doi.org/10.1175/1520-0485(1977)007<0811:APFZFA>2.0.CO;2), 1977.
- 350 Good, S. A., Martin, M. J., and Rayner, N. A.: EN4: Quality controlled ocean temperature and salinity profiles and monthly objective analyses with uncertainty estimates: THE EN4 DATA SET, *Journal of Geophysical Research: Oceans*, 118, 6704–6716, <https://doi.org/10.1002/2013JC009067>, 2013.
- Gouretski, V. and Cheng, L.: Correction for systematic errors in the global dataset of temperature profiles from mechanical bathythermographs, *Journal of Atmospheric and Oceanic Technology*, 37, 841–855, 2020.
- 355 Gouretski, V. and Reseghetti, F.: On depth and temperature biases in bathythermograph data: Development of a new correction scheme based on analysis of a global ocean database, *Deep Sea Research Part I: Oceanographic Research Papers*, 57, 812–833, 2010.
- Graham, R. M., de Boer, A. M., Heywood, K. J., Chapman, M. R., and Stevens, D. P.: Southern Ocean fronts: Controlled by wind or topography?: SOUTHERN OCEAN FRONTS IN HIGEM, *Journal of Geophysical Research: Oceans*, 117, n/a–n/a, <https://doi.org/10.1029/2012JC007887>, 2012.
- 360 Helber, R. W., Kara, A. B., Richman, J. G., Carnes, M. R., Barron, C. N., Hurlburt, H. E., and Boyer, T.: Temperature versus salinity gradients below the ocean mixed layer: TEMPERATURE VERSUS SALINITY GRADIENTS, *Journal of Geophysical Research: Oceans*, 117, n/a–n/a, <https://doi.org/10.1029/2011JC007382>, 2012.
- Johnson, G. C., Kunze, E., McTaggart, K. E., and Moore, D. W.: Temporal and Spatial Structure of the Equatorial Deep Jets in the Pacific Ocean*, *Journal of Physical Oceanography*, 32, 3396–3407, [https://doi.org/10.1175/1520-0485\(2002\)032<3396:TASSOT>2.0.CO;2](https://doi.org/10.1175/1520-0485(2002)032<3396:TASSOT>2.0.CO;2), 365 2002.
- Johnson, G. C., Schmidtko, S., and Lyman, J. M.: Relative contributions of temperature and salinity to seasonal mixed layer density changes and horizontal density gradients: GLOBAL SEASONAL MIXED LAYER T AND S ROLES, *Journal of Geophysical Research: Oceans*, 117, n/a–n/a, <https://doi.org/10.1029/2011JC007651>, 2012.
- Karstensen, J.: Formation of the South Pacific Shallow Salinity Minimum: A Southern Ocean Pathway to the Tropical Pacific, *Journal of Physical Oceanography*, 34, 2398–2412, <https://doi.org/10.1175/JPO2634.1>, 2004. 370
- Martin, T., Park, W., and Latif, M.: Multi-centennial variability controlled by Southern Ocean convection in the Kiel Climate Model, *Climate Dynamics*, 40, 2005–2022, <https://doi.org/10.1007/s00382-012-1586-7>, 2013.
- Martinson, D. G., Killworth, P. D., and Gordon, A. L.: A Convective Model for the Weddell Polynya, *Journal of Physical Oceanography*, 11, 466–488, [https://doi.org/10.1175/1520-0485\(1981\)011<0466:ACMFTW>2.0.CO;2](https://doi.org/10.1175/1520-0485(1981)011<0466:ACMFTW>2.0.CO;2), 1981.
- 375 Pauthenet, E., Roquet, F., Madec, G., and Nerini, D.: A Linear Decomposition of the Southern Ocean Thermohaline Structure, *Journal of Physical Oceanography*, 47, 29–47, <https://doi.org/10.1175/JPO-D-16-0083.1>, 2017.

- Pellichero, V., Sallée, J.-B., Schmidtko, S., Roquet, F., and Charrassin, J.-B.: The ocean mixed layer under Southern Ocean sea-ice: Seasonal cycle and forcing: OCEAN MIXED LAYER UNDER SOUTHERN SEA-ICE, *Journal of Geophysical Research: Oceans*, 122, 1608–1633, <https://doi.org/10.1002/2016JC011970>, 2017.
- 380 Perovich, D. K. and Polashenski, C.: Albedo evolution of seasonal Arctic sea ice, *Geophysical Research Letters*, 39, 2012GL051432, <https://doi.org/10.1029/2012GL051432>, 2012.
- Pierce, D. W., Barnett, T. P., and Mikolajewicz, U.: Competing Roles of Heat and Freshwater Flux in Forcing Thermohaline Oscillations, *Journal of Physical Oceanography*, 25, 2046–2064, [https://doi.org/10.1175/1520-0485\(1995\)025<2046:CROHAF>2.0.CO;2](https://doi.org/10.1175/1520-0485(1995)025<2046:CROHAF>2.0.CO;2), 1995.
- Pollard, R., Lucas, M., and Read, J.: Physical controls on biogeochemical zonation in the Southern Ocean, *Deep Sea Research Part II: Topical Studies in Oceanography*, 49, 3289–3305, [https://doi.org/10.1016/S0967-0645\(02\)00084-X](https://doi.org/10.1016/S0967-0645(02)00084-X), 2002.
- 385 Polyakov, I. V., Pnyushkov, A. V., Rember, R., Padman, L., Carmack, E. C., and Jackson, J. M.: Winter Convection Transports Atlantic Water Heat to the Surface Layer in the Eastern Arctic Ocean*, *Journal of Physical Oceanography*, 43, 2142–2155, <https://doi.org/10.1175/JPO-D-12-0169.1>, 2013.
- Roden, G. I.: Aspects of the Mid-Pacific Transition Zone, *Journal of Geophysical Research*, 75, 1097–1109, <https://doi.org/10.1029/JC075i006p01097>, 1970.
- 390 Roquet, F., Ferreira, D., Caneill, R., Schlesinger, D., and Madec, G.: Unique thermal expansion properties of water key to the formation of sea ice on Earth, *Science Advances*, 8, <https://doi.org/10.1126/sciadv.abq0793>, 2022.
- Sallée, J.-B., Speer, K., Rintoul, S., and Wijffels, S.: Southern Ocean Thermocline Ventilation, *Journal of Physical Oceanography*, 40, 509–529, <https://doi.org/10.1175/2009JPO4291.1>, 2010.
- 395 Sallée, J.-B., Pellichero, V., Akhoudas, C., Pauthenet, E., Vignes, L., Schmidtko, S., Garabato, A. N., Sutherland, P., and Kuusela, M.: Summertime increases in upper-ocean stratification and mixed-layer depth, *Nature*, 591, 592–598, <https://doi.org/10.1038/s41586-021-03303-x>, 2021.
- Schmidtko, S., Johnson, G. C., and Lyman, J. M.: MIMOC: A global monthly isopycnal upper-ocean climatology with mixed layers: MIMOC, *Journal of Geophysical Research: Oceans*, 118, 1658–1672, <https://doi.org/10.1002/jgrc.20122>, 2013.
- 400 Schmitt, R. W.: Double Diffusion in Oceanography, *Annual Review of Fluid Mechanics*, 26, 255–285, <https://doi.org/10.1146/annurev.fl.26.010194.001351>, 1994.
- Sokolov, S. and Rintoul, S. R.: Circumpolar structure and distribution of the Antarctic Circumpolar Current fronts: I. Mean circumpolar paths, *Journal of Geophysical Research*, 114, C11018, <https://doi.org/10.1029/2008JC005108>, 2009.
- Sterl, M. F. and De Jong, M. F.: Restratification Structure and Processes in the Irminger Sea, *Journal of Geophysical Research: Oceans*, 127, [e2022JC019126](https://doi.org/10.1029/2022JC019126), <https://doi.org/10.1029/2022JC019126>, 2022.
- 405 Stern, M. E.: The “Salt-Fountain” and Thermohaline Convection, *Tellus*, 12, 172–175, <https://doi.org/10.3402/tellusa.v12i2.9378>, 1960.
- Stewart, K. D. and Haine, T. W. N.: Thermobaricity in the Transition Zones between Alpha and Beta Oceans, *Journal of Physical Oceanography*, 46, 1805–1821, <https://doi.org/10.1175/JPO-D-16-0017.1>, 2016.
- Thomas, S. D. A., Jones, D. C., Faul, A., Mackie, E., and Pauthenet, E.: Defining Southern Ocean fronts using unsupervised classification, *Ocean Science*, 17, 1545–1562, <https://doi.org/10.5194/os-17-1545-2021>, 2021.
- 410 Trathan, P. N., Brandon, M. A., and Murphy, E. J.: Characterization of the Antarctic Polar Frontal Zone to the north of South Georgia in summer 1994, *Journal of Geophysical Research: Oceans*, 102, 10483–10497, <https://doi.org/10.1029/97JC00381>, 1997.
- Treguier, A. M., de Boyer Montégut, C., Bozec, A., Chassignet, E. P., Fox-Kemper, B., McC. Hogg, A., Iovino, D., Kiss, A. E., Le Sommer, J., Li, Y., Lin, P., Lique, C., Liu, H., Serazin, G., Sidorenko, D., Wang, Q., Xu, X., and Yeager, S.: The mixed-layer depth in the

- 415 Ocean Model Intercomparison Project (OMIP): impact of resolving mesoscale eddies, *Geoscientific Model Development*, 16, 3849–3872, <https://doi.org/10.5194/gmd-16-3849-2023>, 2023.
- You, Y.: A global ocean climatological atlas of the Turner angle: implications for double-diffusion and water-mass structure, *Deep Sea Research Part I: Oceanographic Research Papers*, 49, 2075–2093, [https://doi.org/10.1016/S0967-0637\(02\)00099-7](https://doi.org/10.1016/S0967-0637(02)00099-7), 2002.